CHEMISTRY OF MATERIALS
Article

Chem. Mater. **2010,** *22,* 6409–6415 6409
DOI:10.1021/cm1025816

Formation of Nanoparticle-Containing Multilayers in Nanochannels via Layer-by-Layer Assembly

Jun Young Kim,[†,‡] Jonathan P. DeRocher,[§] Pan Mao,[⊥] Jongyoon Han,[#,||] Robert E. Cohen,*[,§] and Michael F. Rubner*[,†]

[†]*Department of Materials Science and Engineering,* [§]*Department of Chemical Engineering,* [⊥]*Department of Mechanical Engineering,* [#]*Department of Electrical Engineering and Computer Science, and* [||]*Department of Biological Engineering, Massachusetts Institute of Technology, 77 Massachusetts Avenue, Cambridge, Massachusetts 02139, United States, and* [‡]*Corporate Research & Development Center, Samsung SDI Co. Ltd., 428-5, Gongse-dong, Giheung-gu, Yongin-si, Gyeonggi-do, 446-577, Republic of Korea*

Received September 8, 2010. Revised Manuscript Received October 20, 2010

Arrays of silicon nanochannels were used to investigate the layer-by-layer (LbL) assembly of nanoparticle-containing multilayers in confined geometries. LbL assembly of poly(vinylsulfonic acid)/titania (PVS/TiO_2) and poly(diallyldimethylammonium chloride)/silica ($PDAC/SiO_2$) resulted in conformal, uniform thickness multilayers throughout the high-aspect-ratio nanochannels. These multilayers were also calcinated to form nanoporous coatings within the nanochannels. Confined and unconfined multilayers were compared using scanning electron microscopy (SEM), showing significantly lower bilayer thicknesses when layers were assembled in confined geometries. Deposition was found to essentially stop at a nanochannel gap size of 55 nm for the PVS/TiO_2 system and at 210 nm for the $PDAC/SiO_2$ system, even though the channels were not plugged. These results provide further evidence of surface charge-induced depletion of unadsorbed species during LbL assembly, which occurs because of the closely spaced walls with like surface charge inherent in confined geometry LbL. This approach offers a simple but powerful new pathway to functionalize nanochannels with nanoporous coatings made from LbL-assembled nanoparticle-containing multilayers. It has applications in the production of functionalized nanofluidic devices for advanced separations utilizing size, charge, and potentially chemical or biological selectivity.

Introduction

Recently, nanofluidic devices comprising channels with at least one nanoscale dimension have attracted growing interest due to their high throughput, small volume of reactants, and fast kinetics.[1−3] To achieve high efficiency, good repeatability, and multiple functionality in these devices, several strategies for functionalization of the channel surfaces have been implemented including physical adsorption, dynamic coating, and permanent surface modification by covalent linkage or cross-linking.[4−8] Another promising technique is the use of layer-by-layer (LbL) assembly to fabricate multilayer films by alternate deposition of oppositely charged species. LbL assembly is a simple and versatile approach for the fabrication of molecular assemblies of tailored architectures with multiple functionalities, allowing precise control of the thickness, composition, and physical/chemical properties of multilayered composite films on the nanoscale level.[9−11]

Previous papers from our laboratory and others have reported successful LbL assembly of charged macromolecules in confined geometries.[12−22] Conformal, ionically cross-linked, polymeric coatings with attractive features

*Corresponding author. E-mail: rubner@mit.edu (M.F.R.); recohen@mit.edu (R.E.C.).

(1) Han, J.; Craighead, H. G. *Science* **2000**, *288*, 1026–1029.
(2) Huh, D.; Mills, K. L.; Zhu, X.; Burns, M. A.; Thouless, M. D.; Takayama, S. *Nat. Mater.* **2007**, *6*, 424–428.
(3) Abgrall, P.; Nguyen, N. T. *Anal. Chem.* **2008**, *80*, 2326–2341.
(4) Makamba, H.; Kim, J. H.; Lim, K.; Park, N.; Hahn, J. H. *Electrophoresis* **2003**, *24*, 3607–3619.
(5) Liu, J.; Lee, M. L. *Electrophoresis* **2006**, *27*, 3533–3546.
(6) Horvath, J.; Dolník, V. *Electrophoresis* **2001**, *22*, 644–655.
(7) Baxamusa, S. H.; Gleason, K. K. *Chem. Vap. Deposition* **2008**, *14*, 313–318.
(8) Ozaydin-Ince, G.; Gleason, K. K. *Chem. Vap. Deposition* **2010**, *16*, 100–105.
(9) Decher, G. *Science* **1997**, *277*, 1232–1237.
(10) Esker, A. R.; Mengel, C.; Wegner, G. *Science* **1998**, *280*, 892–895.
(11) Caruso, F.; Caruso, R. A.; Möhwald, H. *Science* **1998**, *282*, 1111–1114.
(12) Lee, D.; Nolte, A. J.; Kunz, A. L.; Rubner, M. F.; Cohen, R. E. *J. Am. Chem. Soc.* **2006**, *128*, 8521–8529.
(13) DeRocher, J. P.; Mao, P.; Han, J.; Rubner, M. F.; Cohen, R. E. *Macromolecules* **2010**, *43*, 2430–2437.
(14) Chia, K.-K.; Rubner, M. F.; Cohen, R. E. *Langmuir* **2009**, *25*, 14044–14052.
(15) Lee, D.; Cohen, R. E.; Rubner, M. F. *Langmuir* **2007**, *23*, 123–129.
(16) Wang, Y.; Angelatos, A. S.; Caruso, F. *Chem. Mater.* **2008**, *20*, 848–858.
(17) Wang, Y.; Angelatos, A. S.; Dunstan, D. E.; Caruso, F. *Macromolecules* **2007**, *40*, 7594–7600.
(18) Angelatos, A. S.; Wang, Y.; Caruso, F. *Langmuir* **2008**, *24*, 4224–4230.
(19) Arsenault, A. C.; Halfyard, J.; Wang, Z.; Kitaev, V.; Ozin, G. A.; Manners, I.; Mihi, A.; Miguez, H. *Langmuir* **2005**, *21*, 499–503.
(20) Ai, S.; Lu, G.; He, Q.; Li, J. *J. Am. Chem. Soc.* **2003**, *125*, 11140–11141.
(21) Hou, S.; Harrell, C. C.; Trofin, L.; Kohli, P.; Martin, C. R. *J. Am. Chem. Soc.* **2004**, *126*, 5674–5675.
(22) Ali, M.; Yameen, B.; Cervera, J.; Ramírez, P.; Neumann, R.; Ensinger, W.; Knoll, W.; Azzaroni, O. *J. Am. Chem. Soc.* **2010**, *132*, 8338–8348.

Published on Web 11/08/2010

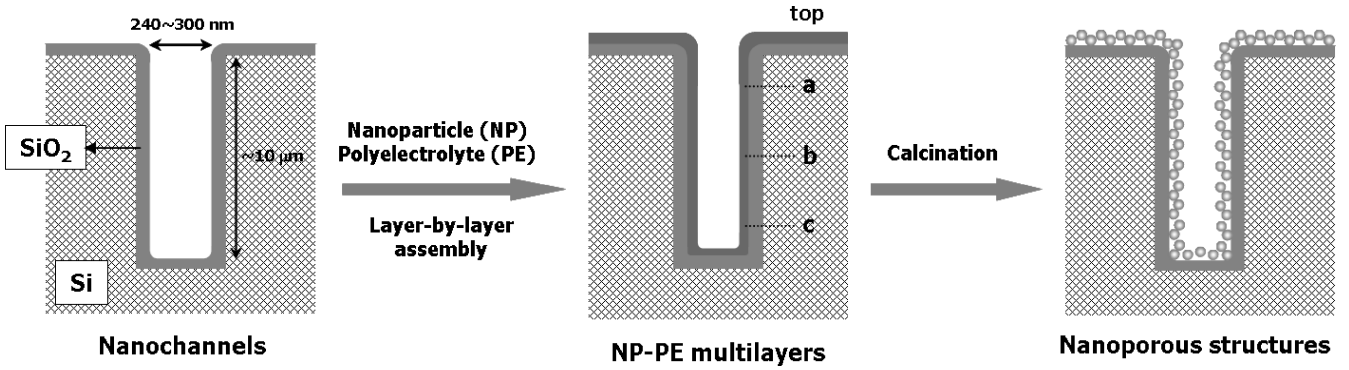

Figure 1. Schematic drawing of LbL assembly of nanoporous coatings within a nanochannel. Nanoparticle-containing multilayers are assembled in nanochannels via sequential deposition of charged nanoparticles and polyelectrolytes. Subsequent calcination of the precursor film results in the formation of nanoporous structures in the nanochannels. Nanoparticle-containing multilayers deposited in nanochannels show uniform thickness distribution over the (a) upper, (b) middle, and (c) lower parts of the nanochannels.

such as dimensional responsiveness to pH changes and adjustable surface charge and surface chemistry have been produced on the inner walls of templates with submicrometer geometric features. Successful LbL processing was achieved even when one of the characteristic dimensions of the coated template decreased to the same order of magnitude as the macromolecular coil dimensions, i.e., in the regime of tens of nanometers.

Here we extend these previous studies to include LbL assembly of charged nanoparticles in confined geometries. We have studied various oppositely charged polymer−nanoparticle pairs, and we report on two specific systems that demonstrate the issues and opportunities that arise in confined geometry LbL assembly: positively charged TiO_2 nanoparticles partnered with poly(vinylsulfonic acid) (PVS) and poly(diallyldimethylammonium chloride) (PDAC) partnered with negatively charged SiO_2 nanoparticles. The latter system was first studied in detail by Lvov et al.[23] The selection of Si/SiO_2 nanochannel templates[24] provides the opportunity to use high-temperature calcination[25] to remove the organic material from the LbL film, leaving a nanoporous inorganic layer of adjustable thickness on the walls of the template. Such nanoporous coatings add a new dimensional element to the functionalization of nanochannel arrays and may allow the implementation of nanoscale selective permeation effects similar to those exploited in size exclusion chromatography. Figure 1 provides a schematic summary of this approach.

Experimental Methods

High-aspect-ratio nanochannel arrays were fabricated according to procedures described in detail elsewhere.[24] The long rectangular trenches varied in initial width from about 240−300 nm, with depths of about 10 μm. Silicon wafers (WaferNet, Inc.) were used as control planar substrates. PVS (25 wt % solution in water, $M_w = 4000-5000$ g/mol), poly(allylamine hydrochloride) (PAH, $M_w = 56\,000$ g/mol) poly(sodium 4-styrenesulfonate) (PSS, $M_w = 70\,000$ g/mol), and PDAC (35% solution in water, $M_w \approx 10\,000$ g/mol) were purchased from Sigma-Aldrich (St. Louis, MO) and used as received. TiO_2 nanoparticles (mean particle size *ca.* 6 nm) were synthesized and characterized according to procedures described elsewhere.[26] SiO_2 nanoparticles (Ludox HS-40, average particle size ca. 15 nm) were purchased from Sigma-Aldrich (St. Louis, MO). Deionized water (18.2 MΩ.cm, Millipore Milli-Q) was used in all aqueous solutions and rinse baths. Each solution was adjusted to the desired pH value with nitric acid for TiO_2/PVS and with hydrochloric acid or sodium hydroxide for PDAC/SiO_2. Unless otherwise specified, the concentrations of nanoparticles and polyelectrolytes in the dipping solutions were 0.015 wt % and 0.01 M (repeat unit basis), respectively.

Substrates were cleaned by three 10 min sonication steps in a detergent solution (3% Micro-90, International Products Corp.), 1 M hydrochloric acid, and deionized water. After thorough rinsing with deionized water, the cleaned substrates were blow-dried with compressed air. Not adhering to these cleaning steps led to nonuniform multilayers and aggregation/blockage in the nanochannels. LbL processing was performed using a Strato-Sequence VI spin dipper (nanoStrata, Inc.). The dipping time in each solution was 15 min followed by three intermediate rinsing steps (3, 2, and 1 min) in pH adjusted deionized water. In all cases, the substrates were spun at 120 rpm. Multilayers of poly(vinylsulfonic acid)/titania (PVS/TiO_2) were assembled at pH 1.5, whereas poly(diallyldimethylammonium chloride)/silica (PDAC/SiO_2) multilayers were assembled at pH 9.0

Calcination was performed at 550 °C for 2 h using a Barnstead Thermolyne 47900 furnace to remove organic polymer. Upon completion of the calcination process, the furnace was shut off and the coated nanochannel arrays were allowed to cool in the oven until ambient temperature was reached. The thicknesses of nanoparticle−polymer films and of calcinated nanoparticle films on flat silicon substrates were measured using spectroscopic ellipsometry (XLS-100, J. A. Woolam Co., Inc.) according to procedures described in detail elsewhere.[27,28] High resolution scanning electron microscopy (HR-SEM) was used to measure the thicknesses of multilayers deposited in the nanochannels and on the unconfined top surfaces of the nanochannel arrays. HR-SEM micrographs were obtained using a JEOL 6320 operated at an accelerating voltage of 5 kV.

(23) Lvov, Y.; Ariga, K.; Onda, M.; Ichinose, I.; Kunitake, T. *Langmuir* **1997**, *13*, 6195–6203.
(24) Mao, P.; Han, J. *Lab Chip* **2009**, *9*, 586–591.
(25) Cebeci, F. C.; Wu, Z.; Zhai, L.; Cohen, R. E.; Rubner, M. F. *Langmuir* **2006**, *22*, 2856–2862.
(26) Choi, W.; Termin, A.; Hoffmann, M. R. *J. Phys. Chem.* **1994**, *98*, 13669–13679.
(27) Lee, D.; Rubner, M. F.; Cohen, R. E. *Nano Lett.* **2006**, *6*, 2305–2312.
(28) Lee, D.; Omolade, D.; Cohen, R. E.; Rubner, M. F. *Chem. Mater.* **2007**, *19*, 1427–1433.

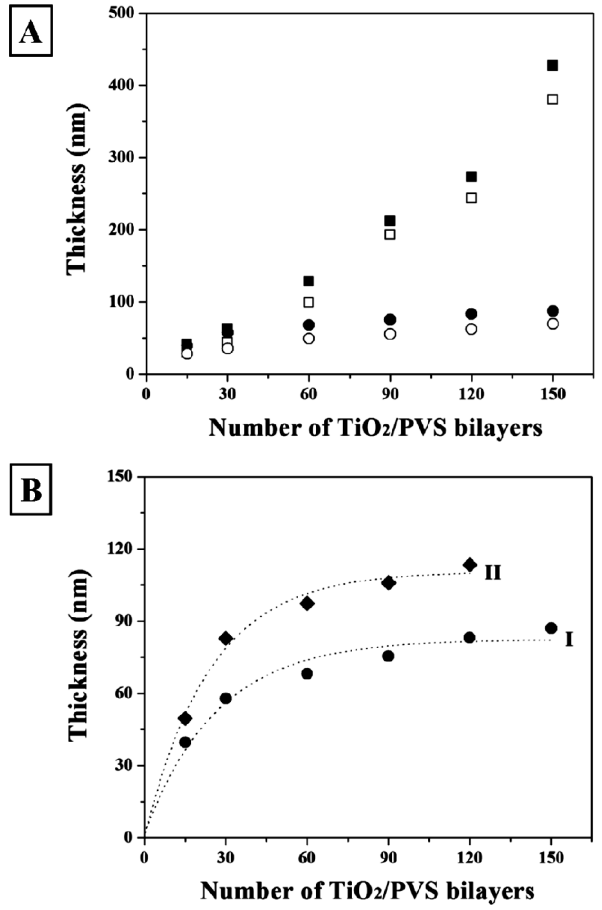

Figure 2. (A) Thickness of TiO_2/PVS multilayers deposited at pH 1.5 with no added salt on the top surface (squares) and nanochannel walls (circles) as a function of the number of deposited TiO_2/PVS bilayers. Filled and open symbols represent the thickness of as-assembled and calcinated films, respectively. (B) Growth behavior of TiO_2/PVS multilayers (I, repeated from 2A) without and (II) with a 5 bilayer PAH/PSS adhesion layer on the nanochannel walls as a function of the number of deposited TiO_2/PVS bilayers. The thickness of the film in (II) includes the thickness of the adhesion layer, which is about 2−3 nm thick. The dotted lines are the best fit exponential decay curves, $a = a_0[1 - \exp(-x/x_0)]$. The parameters obtained from the best fits are $a_0 = 80.7$ nm and $x_0 = 26.7$ bilayers for TiO_2/PVS and $a_0 = 110.6$ nm and $x_0 = 24.0$ bilayers for TiO_2/PVS with a PAH/PSS adhesion layer.

Results and Discussion

TiO_2/PVS System. Herein we describe the fabrication of nanochannels functionalized with conformal, uniform TiO_2/PVS multilayers via electrostatic LbL assembly and nanoporous titania films formed by subsequent calcination. TiO_2/PVS multilayers assembled on flat substrates exhibit uniform deposition and linear thickness growth with the number of deposited bilayers (see the Supporting Information, Figure S1). The average bilayer thickness on flat substrates (*ca.* 3.07 nm/bilayer) was smaller than the size of TiO_2 nanoparticles used, which can be explained by isolated domain growth.[29] Figure 2A shows that LbL assembly of TiO_2 and PVS proceeds very differently on the top surface of the nanochannel template compared to the channels themselves. On the top surface, linear growth of the multilayer film persists up to 150 bilayers (~430 nm). The average bilayer thicknesses on the top surface are 2.66 nm/bilayer as-assembled and 2.42 nm/bilayer after calcination. Similar linear growth was observed on the top surface when the nanochannel template was pretreated with a few PAH/PSS adhesion layers (see the Supporting Information, Figures S2 and S3), and the average as-assembled bilayer thickness increased to 2.79 nm/bilayer in this case.

The growth behavior of TiO_2/PVS multilayers assembled on the nanochannel walls is shown in Figure 2B. The coating thickness increased rapidly at first, and then exhibited lower thickness increments as deposition progressed. The thickness of the TiO_2/PVS multilayers on the nanochannel walls was not directly proportional to the number of deposited bilayers, indicating complex, nonlinear growth. The data can be described by an inverted exponential decay with a correlation factor of greater than 0.98 as shown in Figure 2B. These data suggest ultimate film thicknesses of 81 and 111 nm without and with adhesion layers respectively. The final gap thickness is given by $f = f_0 - 2t$ where f_0 is the initial gap thickness and t is the film thickness on each side. According to this formula, the limiting film thicknesses above correspond to final gap thicknesses of about 79 nm since the initial gaps were approximately 240 and 300 nm respectively. In addition, the decay constants are characteristic of the point at which nonlinear growth begins to dominate and the growth of the LbL film slows noticeably in the nanochannels compared to the behavior on the top surface. This general phenomenon, smaller bilayer thickness in the channels, was also observed in our earlier work[13] that involved all-polymer assembly, but it is much more pronounced in the present case. We have proposed two mechanisms for the lower growth rate in the channels: surface charge-induced depletion of unadsorbed polyelectrolytes in the channels and steric rejection of the highest-molecular-weight fraction of the polydisperse macromolecules employed in the LbL assembly. Although the kinetics of transport into the channel may also play a role, as in our earlier work we observe uniform coating thicknesses throughout the high aspect ratio channels indicating that this process is not kinetically limited. For the case of all-polyelectrolyte assemblies, the magnitude of the observed reduction in bilayer thickness in the channels depended on the concentration of any added salt in the process, varying from a factor of 1.8 in the absence of salt to 1.4 when 0.5 M NaCl was added to the dipping solutions. Figure 2 shows that salt-free assembly of the TiO_2/PVS system yields multilayer films on the nanochannel walls that are thinner than the corresponding films assembled free of geometric constraints on the top surfaces by more than a factor of 6 at 150 bilayers.

The SEM micrograph of Figure 3A provides clear visual evidence of the difference in multilayer growth on the top and in the channels of the templates. Despite this reduced growth rate in the channels, the micrographs in Figure 3 also show that the coated channel gaps remain open throughout the assembly process and that the films on the channel walls are of uniform thickness from the top

(29) Ostrander, J. W.; Mamedov, A. A.; Kotov, N. A. *J. Am. Chem. Soc.* **2001**, *123*, 1101–1110.

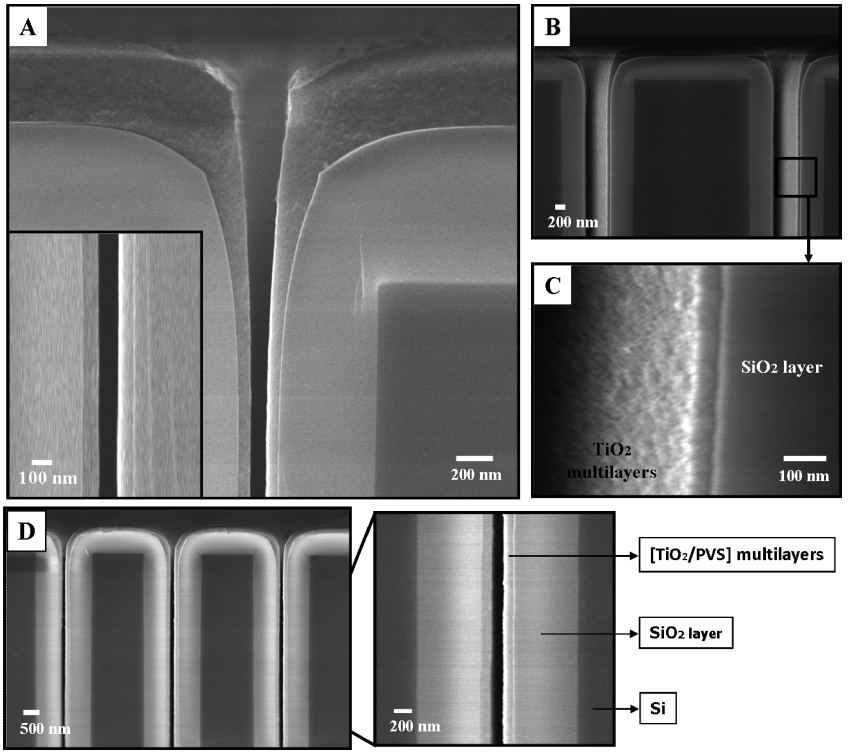

Figure 3. (A) HR-SEM micrograph showing a cross-sectional view of the nanochannels coated with 120 bilayers of TiO_2/PVS. The inset shows a magnified view of the uniform, conformal multilayer within the nanochannel. (B) HR-SEM micrograph of the nanochannels coated with a 90 bilayer TiO_2/PVS multilayer after calcination. (C) Highly magnified view of Figure 3B showing a nanoporous titania film on a nanochannel wall. (D) Cross-sectional HR-SEM micrographs of the nanochannels coated with 90 bilayers of TiO_2/PVS showing uniform coating throughout the nanochannel.

to the bottom of the 10 μm deep channels (Figure 3D). These observations suggest that TiO_2 nanoparticle aggregation is not a significant problem under the conditions specified. The surface roughness of the films on the channel walls (Figure 3C) is similar to what is seen for films assembled in the absence of geometric constraint. Finally, high-temperature calcination leads to conformally adherent nanoporous titania coatings on the walls of the channels with no visible defects, indicating that calcination does not damage the film or the underlying template (Figure 3B).

The dependence of the confined TiO_2/PVS multilayer thickness on deposition concentration was investigated and the results show that thicker films are obtained when either the PVS or TiO_2 nanoparticle concentrations are increased (see the Supporting Information, Figure S4). Cross-sectional HR-SEM images show uniform, conformal coating of the nanochannels before and after calcination (see the Supporting Information, Figure S5). These results suggest that we can control the bilayer thickness of TiO_2/PVS multilayers in nanochannels by varying the concentration of the deposition solutions without compromising coating uniformity.

A more detailed analysis of the influence of channel confinement on film growth is shown in Figure 4. Figure 4A shows the residual channel gap as a function of the number of LbL-processed bilayers. Figure 4B shows how the wall/top thickness ratio varies as LbL processing proceeds. In Figure 4C the nominal growth rate of the films becomes an approximately linear function of the inverse gap size below dimensions of about 100 nm; extrapolation suggests that confinement at a gap dimension of about 55 nm is sufficient to effectively stop the LbL assembly process in the channels for the TiO_2/PVS system. The 6 nm diameter TiO_2 nanoparticles are significantly smaller than this critical gap size, and the length of the fully extended configuration of a 40-unit PVS chain is only about 10 nm. It therefore seems unlikely that geometric exclusion of the constituents of the TiO_2/PVS system is responsible for the diminishing assembly rates in the channels. Thus, as suggested in our earlier study[13] of all-polymer assembly in nanochannels, it appears that the presence of surface charge on the channel walls[30] provides a sufficient level of electrostatic repulsion over the full width of the channel to deplete the supply of adsorbing species needed for LbL growth on the channel walls.

PDAC/SiO_2 System. To demonstrate that the above results are generalizable, we also performed LbL assembly of PDAC/SiO_2 in nanochannels and used calcination to form conformal, nanoporous silica films. Unconfined assembly of PDAC/SiO_2 resulted in uniform deposition and thickness growth which was linear with respect to the number of deposited bilayers (see the Supporting Information, Figure S6). As with the TiO_2/PVS multilayers, the average unconfined as-assembled bilayer thickness (ca. 9.89 nm/bilayer) was smaller than the diameter of the SiO_2 nanoparticles used. The refractive index and porosity

(30) Böhmer, M. R.; Evers, O. A.; Scheutjens, J. M. H. M. *Macromolecules* **1990**, *23*, 2288–2301.

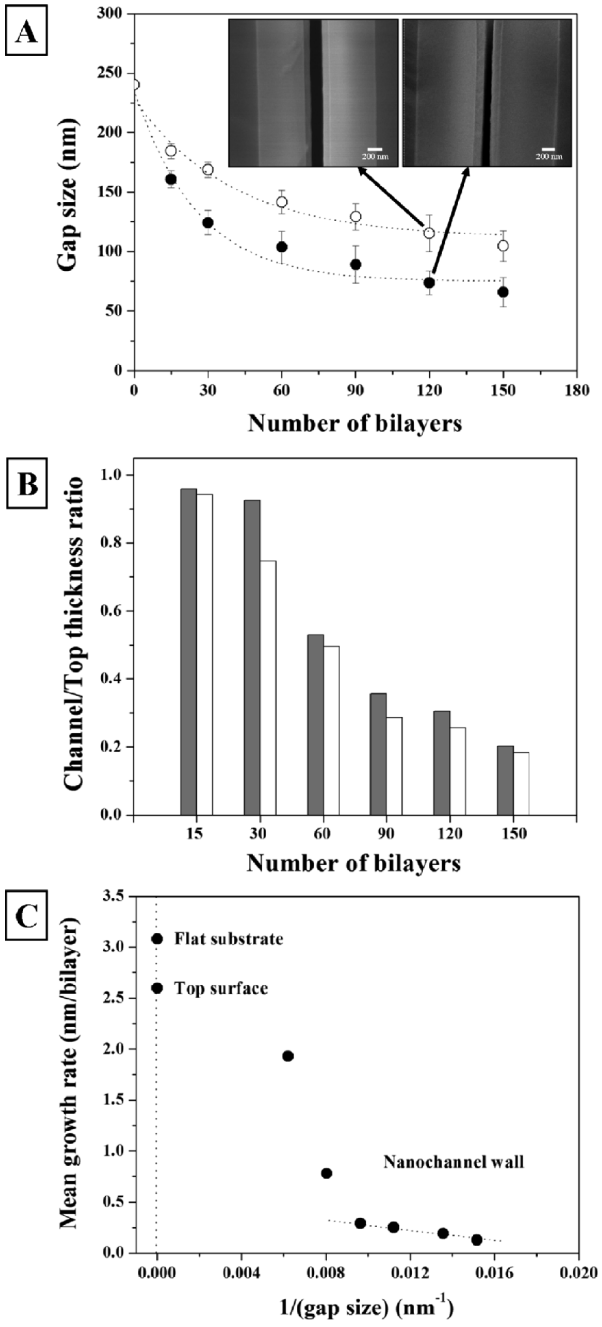

Figure 4. (A) Gap size of nanochannels coated with TiO_2/PVS multilayers as-assembled (filled) and after calcination (open) as a function of the number of deposited TiO_2/PVS bilayers. The insets show cross-sectional views of the nanochannel walls coated with 120 bilayers of TiO_2/PVS (Scale bars: 200 nm). (B) Ratio of the film thickness in the nanochannel to that on the top surface for as-assembled (filled) and calcinated (open) TiO_2/PVS multilayers as a function of the number of deposited TiO_2/PVS bilayers. (C) Comparison of the mean growth rate of TiO_2/PVS multilayers deposited in nanochannels and on flat substrates. The dotted line represents a linear fit of the last four data points as a function of the inverse gap size.

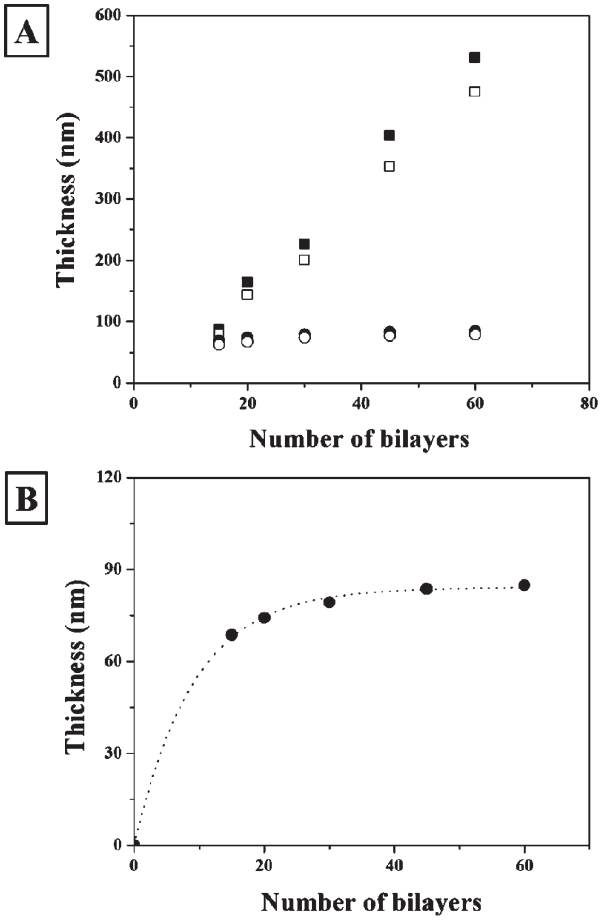

Figure 5. (A) Thickness of PDAC/SiO_2 multilayers deposited at pH 9.0 with no added salt on the top surface (squares) and nanochannel wall (circles) as a function of the number of deposited bilayers. Filled and open symbols represent the thickness of as-assembled and calcinated films, respectively. (B) Growth behavior of PDAC/SiO_2 multilayers on the nanochannel walls as a function of the number of deposited bilayers. The dotted line is the best fit exponential decay curve $a = a_0[1 - \exp(-x/x_0)]$. The parameters obtained from the best fit are $a_0 = 84.1$ nm and $x_0 = 9.2$ bilayers.

of calcinated PDAC/SiO_2 multilayer films were measured using spectroscopic ellipsometry. The refractive indices of PDAC/SiO_2 films were about 1.28−1.29 independent of the number of deposited bilayers (see the Supporting Information, Figure S7) and the porosity was estimated to be ~38%. The nanoporous structure of calcinated PDAC/SiO_2 multilayer films results from the rearrangement and close-packing of silica nanoparticles after removal of polymers.[27,28,31] Figure 5A shows that, similar to TiO_2/PVS, LbL assembly of the PDAC/SiO_2 multilayers within the nanochannel template differs significantly from that on an unconfined surface. On planar surfaces, linear growth persists up to 60 bilayers with average bilayer thicknesses of 9.2 nm/bilayer as-assembled and 8.7 nm/bilayer after calcination. Growth curves for confined PDAC/SiO_2 multilayers are shown in Figure 5B. As before, the data can be described by an inverted exponential decay, with an ultimate film thickness of 84 nm. Figure 5A shows that salt-free assembly of PDAC and SiO_2 yields confined multilayer films that are thinner than the corresponding films assembled free of geometric constraints by more than a factor of 6 at 60 bilayers.

The SEM micrographs of Figure 6 clearly show the thickness contrast between multilayers deposited outside and within the nanochannels. Once again, the channel gaps remain open throughout the assembly process and

(31) Wu, Z.; Lee, D.; Rubner, M. F.; Cohen, R. E. *Small* **2007**, *3*, 1445–1451.

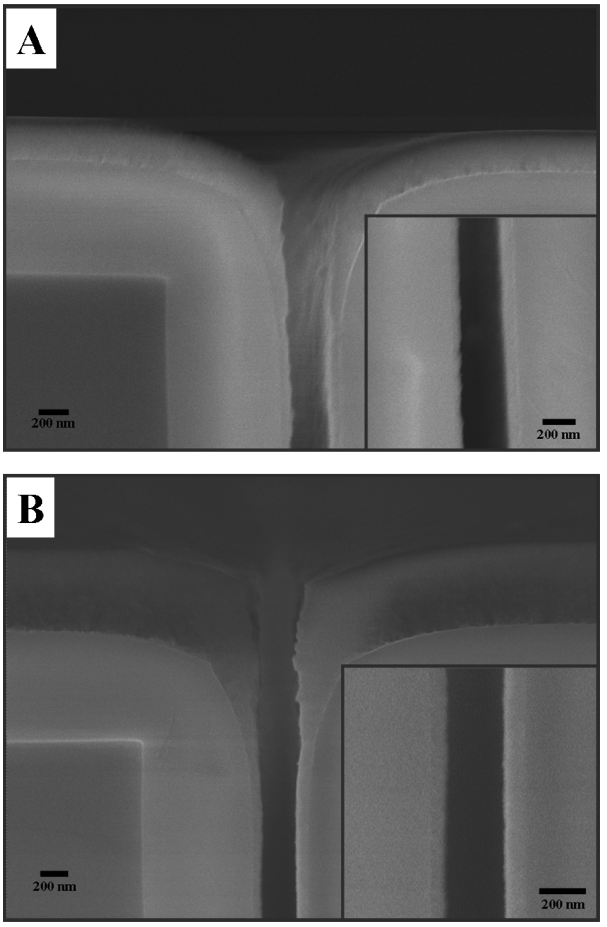

Figure 6. (A) HR-SEM micrograph showing a cross-sectional view of the nanochannels coated with 30 bilayers of PDAC/SiO_2 The inset shows a magnified view of the uniform, conformal multilayer within the nanochannel. (B) HR-SEM micrograph of the nanochannels coated with a 60 bilayer PDAC/SiO_2 film after calcination. The inset is a cross-sectional image showing a conformal film of nanoporous silica throughout the nanochannel after calcination.

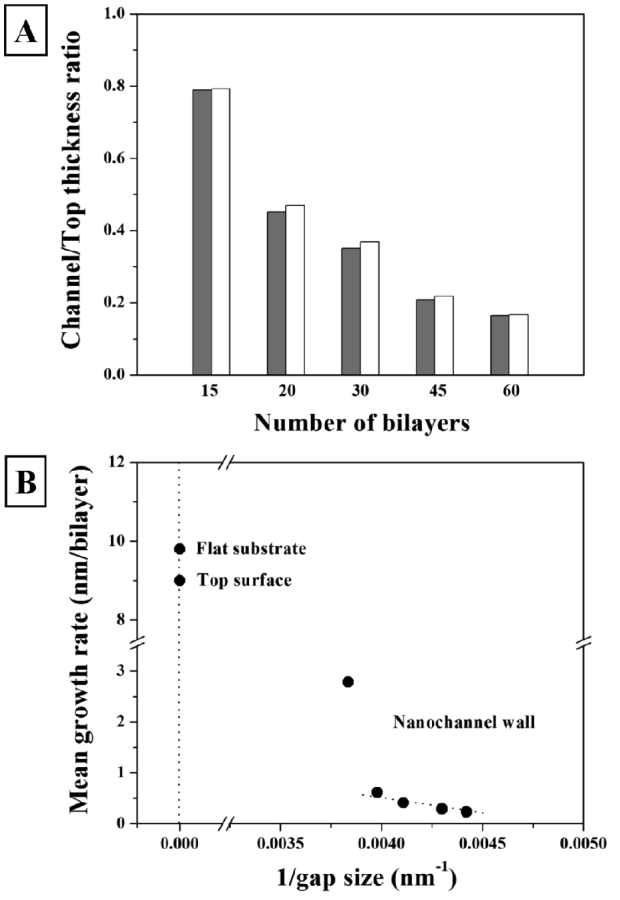

Figure 7. (A) Ratio of the film thickness in the nanochannel wall to that on the top surface for as-assembled (filled) and calcinated (open) PDAC/SiO_2 multilayers as a function of the number of deposited bilayers. (B) Comparison of the mean growth rate of PDAC/SiO_2 multilayers deposited in nanochannels and on flat substrates. The dotted line represents a linear fit of the last four data points as a function of the inverse gap size.

the PDAC/SiO_2 multilayer films on the nanochannel walls are of uniform thickness from the top to the bottom of the channels. High-temperature calcination leads to conformal nanoporous coatings with no visible defects.

Figure 7A shows how the ratio of wall/top film thicknesses varies as LbL deposition proceeds. In Figure 7B, it can be seen that the nominal growth rate of the multilayer becomes an approximately linear function of the inverse gap size, and extrapolation suggests that confinement at a gap of about 210 nm results in no further deposition for the PDAC/SiO_2 system, which is considerably larger than the 55 nm gap obtainable using TiO_2/PVS. This value is significantly bigger than the dimensions of either the nanoparticles or polymer molecules, pointing again to surface charge-induced depletion of unadsorbed species as the likely mechanism.

These two studies show that for two polymer/nanoparticle systems, we have achieved conformal, uniform multilayers with no observable bridging. The only significant difference between the results of these two studies is the significant difference in the lowest achievable gap size. We believe that this difference is attributable to the significantly different ionic strengths of the solutions from which these multilayers were assembled. Although no salt was added in either case, acidic and basic solutions were used to adjust the pH of each solution to the desired value. In the TiO_2/PVS case, the pH was 1.5 implying an ionic strength of about 0.03 M, whereas in the PDAC/SiO_2 case, the pH was 9 and the ionic strength was on the order of 1×10^{-5} M. The limiting gap sizes for these systems are 55 and 210 nm respectively. For comparison, in our earlier work on PAH/PSS we achieved gap sizes of about 25 nm at an ionic strength of 0.1 M.[13] These data are consistent with our proposed growth limitation mechanism of exclusion within the nanochannels. At low ionic strength, the wall surface charge is not as well screened, resulting in exclusion of charged species at higher gap sizes.

Ali et al. have also observed that confined LbL assembly of charged species results in interesting phenomena which differ from those found on a flat surface.[22] They measured $I-V$ curves of track etched polycarbonate membranes containing asymmetric pores and observed rectification of ionic current. They fit these results to a Poisson-Nernst-Planck model to calculate the surface charge within the pore. They then assembled multilayer films of PAH and PSS within these pores and, assuming a constant LbL growth rate obtained from the literature,

determined the dependence of surface charge on multilayer growth. They concluded that the surface charge of confined multilayers decreases as deposition proceeds and attributed this effect to ion pairing within the film. This proposed phenomenon could be another explanation for why we observe lower bilayer thicknesses as the gap size becomes smaller. It should be noted, however, that exclusion of charged species within the gap would also result in reduced charge overcompensation in agreement with Ali's results.

Summary and Conclusions

In this work we have used LbL assembly of TiO_2/PVS and PDAC/SiO_2 multilayers to conformally and uniformly coat high-aspect-ratio nanochannel arrays with polymer/nanoparticle composite multilayers and with nanoporous inorganic films. The multilayer thickness and therefore the nanochannel gap size can be tuned systematically by controlling the number of deposited bilayers. LbL assembly of TiO_2/PVS from solutions containing no added salt was successfully achieved down to gaps of below 80 nm and may be possible down to 55 nm. Films deposited on unconfined surfaces were significantly thicker than those deposited within the channels. These results support the idea that surface charge-induced depletion of unadsorbed species in confined geometries limits the growth of LbL assembled thin films within narrow channels, especially at low ionic strengths. The ability to functionalize high-aspect-ratio nanochannels with conformal, nanoporous, inorganic films has numerous applications including micro/nanofluidic reactors and separators or sensors based on size, charge, and potentially chemical or biological selectivity.

An interesting extension of this work is the feasibility of using LbL to fabricate all-nanoparticle multilayers. On the basis of preliminary experimental results, uniform and conformal films formed solely by LbL deposition of nanoparticles have been demonstrated, and detailed studies of these systems are currently underway in our laboratory.

Acknowledgment. This work was supported in part by the MRSEC Program of the National Science Foundation (NSF) under Award DMR-0819762. The authors thank the MRSEC Shared Experimental Facilities and the Institute for Soldier Nanotechnologies (ISN) for use of characterization facilities.

Supporting Information Available: Growth curves for TiO_2/PVS on planar Si substrates, HR-SEM micrographs and plots comparing confined and unconfined deposition of TiO_2/PVS with PAH/PSS adhesion layers, plots and SEM micrographs showing the effect of PVS and TiO_2 deposition solution concentration on TiO_2/PVS multilayer thickness, growth curves for PDAC/SiO_2 on planar Si substrates, and plots showing the refractive index of calcinated PDAC/SiO_2 films (PDF). This material is available free of charge via the Internet at http://pubs.acs.org.